Combinatorial Optimization of Ternary Pt Alloy Catalysts for the Electrooxidation of Methanol

Peter Strasser*

Department of Chemical and Biomolecular Engineering, University of Houston, Houston, Texas 77204-4004

Received October 18, 2007

We report the combinatorial and high-throughput optimization of improved ternary Pt alloy electrocatalysts for the oxidation of methanol for use in direct methanol fuel cell (DMFC) anodes. Following up on the discovery of a ternary $Pt_{20}Co_{60}Ru_{20}$ catalyst[1] with significantly improved electrocatalytic activity for methanol oxidation over standard Pt−Ru catalysts, we optimize the electrocatalytic activity of this composition using a closely sampled Pt−Co−Ru "optimization library". We also screen for compositional and structural stability using high-throughput methods. Composition−activity maps confirmed improved activity in compositional neighborhood of the $Pt_{20}Co_{60}Ru_{20}$ catalyst. Activity trends of Pt−Ru binary alloys were in excellent agreement with fundamental surface electrochemical studies. Structural and compositional catalyst stability was probed using X-ray diffraction (XRD) and energy dispersive X-ray analysis (EDX). Combination of the stability−composition and activity−composition maps resulted in "consensus maps" pointing to a new optimized ternary alloy electrocatalyst for methanol electrooxidation with an overall composition of $Pt_{18}Co_{62}Ru_{20}$.

1. Introduction

Direct methanol fuel cells (DMFCs) are considered an attractive future electrocatalytic energy conversion technology for low-power applications. Based on the high theoretical specific energy of methanol of about 6 Wh/g, DMFCs offer clear advantages even over the most advanced battery concepts with specific energies in the 0.2 Wh/g range.[2–10]

At the cathode of a DMFC, oxygen is reduced to water, while at the anode of a DMFC, liquid methanol is oxidized to carbon dioxide. Methanol initially adsorbs and stepwise H atoms are stripped which are immediately oxidized to protons. Carbon monoxide is the final product after all H atoms are stripped. Oxygenated surface species are required to oxidatively remove CO from the surface. It is still unclear whether the reaction follows a strictly serial reaction mechanism with CO being the exclusive intermediate on the way to CO_2 or whether reactive intermediates can directly react to CO_2.

Power losses resulting from overpotentials associated with sluggish catalytic reaction rates at the cathode and anode, however, seriously limit the practical output power densities of DMFCs. As a result, there is much opportunity for significant activity improvements through advanced electrocatalyst materials research.

A huge body of literature exists on synthesis, physicochemical characterization, and electrochemical testing of low- and high-surface-area electrocatalysts for the electrooxidation of methanol (for recent reviews, see refs 11–20). The most commonly employed anode methanol-oxidation electrocatalyst in DMFCs consists of a $Pt_{50}Ru_{50}$ alloy. The catalyst is often employed as an unsupported metallic powder with high and therefore costly catalyst weight loadings per geometric surface area of the fuel cell. The identification of a more active methanol oxidation catalyst would improve the performance of DMFCs in terms of output power density and cost effectiveness.

Ternary Pt alloys offer the potential for incremental or even step-change improvements of the catalyst activity compared to single or bimetallic systems. This is because surface or subsurface atoms of additional metals result in modifications of the electronic or structural characteristics of the single or bimetallic alloy surface.[21] However, because the compositional space of three component metal alloys becomes very large, accelerated search and testing strategies for suitable alloy catalyst candidates are required. Combinatorial and high-throughput materials development methods offer an efficient way to appropriately search large chemical parameter spaces.[22–33] Recent reports on experimental combinatorial searches for improved electrocatalysts include work on the oxygen reduction reaction,[34–38] as well as on the hydrogen electrooxidation in the presence of CO.[39] A large body of work was published on the methanol electrooxidation.[1,28,37,40–44] Purely experimental high-throughput catalysis approaches offer rapid empirical mapping of synthesis−structure–activity relationships, yet they often fail to provide fundamental insight into the surface chemistry. In combination with model-based computational search strategies, however, combinatorial materials discovery unfolds its full power for accelerated identification and understanding of new catalysts.[1,45] In a previous study,[1] we had reported the preparation and electrochemical high-throughput screening of a very chemically and stoichiometrically diverse Pt alloy

* E-mail: pstrasser@uh.edu.

10.1021/cc700166p CCC: $40.75
Published on Web 02/08/2008

materials library that lead to the discovery of a highly active $Pt_{20}Ru_{20}Co_{60}$ ternary catalyst compound. In combination with first-principle density functional theory (DFT) calculations, we provided a molecular-level rationale to explain the observed catalytic activity trends.

In the present study, we build on our previous results and report a combinatorial optimization of the activity and stability of Pt−Ru−Co ternary alloy electrocatalysts. We first focus on a combinatorial mapping of composition−reactivity relationships by screening a densely sampled Pt−Ru−Co ternary compositional space. We show that our high-throughput screening activity trends are consistent with earlier fundamental studies of Pt−Ru alloys. In a second step, we focus on a high-throughput evaluation of compositional and structural alloy stability characteristics and use consensus maps between reactivity, composition, and stability for a final electrocatalyst selection.

2. Experimental Section

Combinatorial catalyst synthesis and high-throughput electrochemical screening were performed on an array of 64 individually addressable, circular electrodes[1,31,32,46–48] (see Figure 1 in ref 1). Each of the 64 Ti thin film electrode pads is approximately 1.7 mm in diameter (∼0.02 cm^2 area, $A_{geometric}$) and 0.5 μm thick. The electrode pads provide ohmic contacts with the 64 distinct alloy materials to be deposited thereon (referred to as the catalyst "library"). The pads interface the alloy library with a multichannel potentiostat/galvanostat (Arbin Instruments Inc.). The supporting electrodes were made of titanium.

Automated rf-magnetron vacuum sputtering was employed as synthesis methods for Pt alloy films. A moving-shutter technique allowed the controlled deposition of thin-film gradients ranging from a few angstroms to several micrometers. Deposition of multiple different Pt alloy systems with selected compositions (discovery library) was achieved by sputtering multiple metal slabs of onto one or more rows or columns of the array. Smooth compositional variation in the optimization library was achieved by sputtering metal slab with parallel and orthogonal thickness gradients. Typical gradient sputtering steps of an individual metal cover a thickness range from about 5 to 15 Å between, for example, the left and right of the array. Sputtering of superlattice structures (repeat of the sequence of individual metal sputtering) eventually led to the buildup of alloy thin-film thicknesses of up to several thousand angstroms. The deposition conditions were chosen such that the multielement superlattice structures underwent in situ atomic mixing of their individual materials components. X-ray diffraction studies confirmed complete and uniform alloying of the thin films.

For electrochemical testing, the array of electrocatalysts was assembled in a cylindrical cell body such that all 64 electrocatalysts were facing upward and were exposed to the electrolyte at the same time. All contact pads at the edge of the wafer were isolated from the electrolyte using an O-ring seal. A Pt-mesh of about the same circular area as the cross section of the cylindrical cell body was placed in parallel to the quartz wafer at a distance of about 5 cm and served as the common counter electrode. A Hg/Hg_2SO_4 electrode was used as reference electrode. The electrode was sitting in a glass compartment with Luggin−Haber capillary that was filled with base electrolyte. The capillary tip of the reference electrode compartment was placed between the working electrode array and the counter electrode mesh. The distances between the capillary tip of the reference compartment and the working electrodes at the edge and at the center of the array ranged from about 3 to 4 cm. This distance was chosen to be large compared to the distance between individual working electrodes (about 3 mm) to minimize differences in the uncompensated ohmic resistance between catalysts. Voltage drops across the electrolyte between the reference electrode tip and individual working electrodes were considered negligible (on the order of 1−10 μV) given the conductivity and the magnitude of the measured currents. The cell body was further equipped with gas inlet channels for purging the electrolyte with argon, a gastight lid as well as a conventional liquid−seal gas outlet. All potentials in this study will be referred to with respect to the reversible hydrogen scale (RHE) scale with a potential difference of +0.65 V between the two scales at pH 0.

The anode catalysts were electrochemically pretreated using repeated voltammetric cycling of all 64 catalysts between 0–0.7 V/RHE in 0.5 M H_2SO_4 at 20 and 200 mV/s. The pretreatment was stopped as soon as a time-stable voltammogram was obtained for most compositions. Some alloy compositions appeared to continue to change their base voltammetry, especially at large overpotentials, which is likely to indicate corrosive degradation and limited stability of those compositions; those same compositions also exhibit very large hydrogen adsorption integrals. The hydrogen adsorption charge of each catalyst over a potential range of 0.05–0.35 V/RHE on the slow voltammograms was used to estimate the electrochemically active Pt atomic surface area using a hydrogen electrosorption charge density of 210 $\mu C/cm^2$. We note that while this charge density value offers a very accurate mapping between Pt single-crystal surfaces and hydrogen adsorption charges, uncertainties are associated with it when dealing with a Pt alloy surface with non-noble metal atoms in the surface layer on which atomic hydrogen is not underpotentially adsorbed as readily as on Pt. In the latter case, the obtained Pt atomic surface area is considered a lower boundary value. After voltammetric pretreatment, the liquid electrolyte was exchanged with fresh acid to avoid any cross contamination by dissolved metal ions. The pretreated catalyst array was then evaluated with respect to its methanol oxidation activity in a 1 M methanol, 0.5 M sulfuric acid electrolyte. Parallel linear potential scans and parallel chronoamperometric screening (+0.45 V/RHE, 5 min) of all catalysts yielded current density−time curves. All experiments were performed at ambient pressure and room temperature.

Structural and compositional alloy stability was evaluated in high-throughput mode using X-ray diffraction (Siemens D5000 combined with automated $x-y-z$ sample stage and GADDS planar array detector) and SEM/EDX capabilities with automated sample stages. (Hitachi 4300, Oxford EDX).

3. Results and Discussion

A previous combinatorial and high-throughput screening study[1] of ternary methanol electrooxidation catalysts lead to the discovery of an active $Pt_{20}Ru_{20}Co_{60}$ ternary compound. Contrasting experimental activity screenings and computational DFT-based microkinetic activity predictions, we provided a molecular-level rationale in favor of an electronic *ligand effect* of Ru and Co to explain the calculated and experimentally observed trends in CO tolerance and electrocatalytic activity. DFT calculations suggested that the non-Pt atoms modify the electronic structure of Pt surface atoms resulting in a weaker Pt−CO surface bond. This, in turn, leads to lower CO coverages and therefore to a larger number of free Pt surface sites for fuel adsorption and oxidation. Similarly, in case of methanol oxidation, a weaker Pt−CO chemisorption energy may also favor a direct reaction pathway of reactive intermediates to CO_2 via reaction with oxygenated surface species rather than the formation of poisonous surface adsorbed CO.[11,14,49–58]

3.1. Activity Optimization. Library Design. A densely sampled Pt−Co−Ru ternary "optimization library" was synthesized to further optimize the $Pt_{20}Co_{60}Ru_{20}$ catalyst. Figure 1 shows the ternary Pt−Co−Ru compositional space and the individual Pt−Co−Ru compositions sampled by the focus library. Half of the 64 ternary alloy catalysts are spread out evenly over a large portion of the phase space, while the other half are covering a Pt poor portion of the compositional space more densely. A number of alloys are intentionally covering the composition space in the vicinity of the $Pt_{20}Co_{60}Ru_{20}$ composition (lower left corner of ternary diagram). A pure Pt catalyst and a number of Pt−Ru binary alloys were included on the library as benchmarks.

Composition−Activity Trends. The Pt−Co−Ru optimization alloy catalyst library was screened in parallel for catalytic activity in 1 M methanol at various electrode potentials. Activity trends across the ternary compositional space were independent of electrode potential in the potential region studied. The overall alloy catalyst composition often varies from its surface composition because of factors such as incomplete alloying or surface segregation effects.[21,59,60] These factors typically become significant when a thermal annealing step is involved in the alloy synthesis process. This is why many alloy catalysts prepared using liquid metal precursors followed by thermal reduction/annealing show discrepancies between bulk and surface composition. However, studies have repeatedly shown that certain other alloy preparation techniques, such as low-temperature sputtering of thin metal alloy slabs without thermal treatment, show an excellent correlation between initial surface alloy composition and initial bulk alloy composition.[61–67] Given the sputtering technique applied here for the buildup of the alloy library, we are confident that the initial surface compositions are close to the alloy bulk compositions.

Composition−Activity Trends for Pt−Ru Bimetallics. First, the activity trends of Pt−Ru binary alloy catalyst will be considered. Their individual activities are reported in Figure 2. An interesting and surprising trend becomes evident. Under the chosen conditions, the most active Pt−Ru binary alloy is the $Pt_{88}Ru_{12}$ composition with 27 μA/cm2

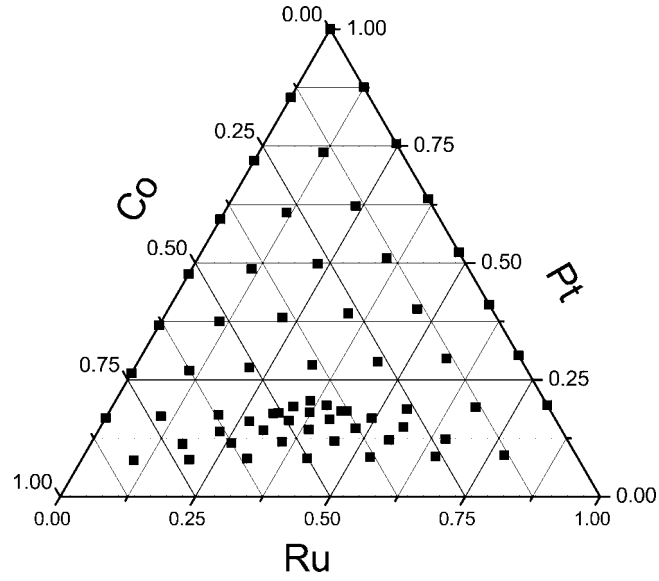

Figure 1. Ternary compositional phase space of the Pt−Co−Ru optimization (focus) library. Black squares indicate the 64 individual ternary compositions which were synthesized and tested on the electrochemical array.

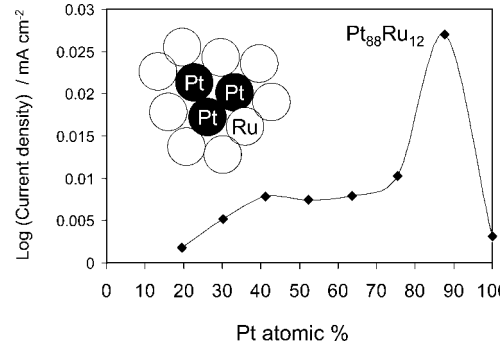

Figure 2. Activity trends of the Pt−Ru binary alloys on the focus library. A maximum for $Pt_{88}Ru_{12}$ was observed. This is consistent with a reactivity model presented in ref 63 where three adjacent Pt atoms and one Ru need to form an ensemble to maximize the catalytic rate (see inset).

after 5 min screening time. The $Pt_{52}Ru_{48}$ alloy is less active, and with increasing Ru content, the activity drops further. While this general trend among Ru-rich compositions is consistent with results from the discovery library, the relative activity between $Pt_{88}Ru_{12}$ and $Pt_{52}Ru_{48}$ deserves some discussion. For methanol oxidation at elevated (about 60 °C) temperatures, the anode electrocatalyst of choice has been a $Pt_{50}Ru_{50}$ catalyst. To explain this, a bifunctional mechanism has traditionally been invoked.[68] Activity enhancements are believed to arise from the atomic scale pairing of Ru atoms and Pt atoms in the surface layer where each metal plays a distinct mechanistic role. Ru atoms have a high affinity for water and OH species, while Pt atoms are preferably covered by strongly adsorbed CO formed from the decomposition of methanol. Because of the direct atomic vicinity of adsorbed OH and CO on an ideal Pt/Ru 1:1 alloy surface, the rate of carbon dioxide is maximized and results in an enhancement of the CO tolerance of the surface and therefore of the overall reaction rate. The results in Figure 2 seem to contradict this bifunctional rational. To explain the current observations one has to keep in mind that the adsorption

characteristics of methanol under the current testing conditions. While methanol adsorbs equally well on Pt or Ru at around 60 C[63] and does not distinguish between Pt and Ru surface sites, methanol does not adsorb readily on Ru atoms under room temperature conditions chosen here.[63] Instead, methanol requires an ensemble of three adjacent Pt surface atoms for its adsorption and subsequent hydrogen stripping toward CO. Once the CO has formed on an ensemble of three Pt atoms, it needs an adjacent Ru atom providing the OH species to complete the reaction (see inset in Figure 2 for the (111) single crystal face). Statistical analysis of single crystal surfaces has shown[63] that the probability of having three adjacent Pt surface atoms next to one Ru atom is maximized at a surface atomic ratio of Pt/Ru of about 92:8, 90:10, and 86:14 for the (111), (100), and (110) single crystals, respectively. Averaging these values for a polycrystalline alloy surface resulted in an optimal atomic ratio of Pt/Ru of 90:10. This model value is in excellent agreement to our alloy composition that exhibits the highest methanol oxidation activity at room temperature. Our results are also consistent with an earlier study on binary and ternary methanol electrooxidation catalysts by Cooper and Ginn.[44] The authors show that at room temperature, a Pt−Ru alloy with overall composition $Pt_{90}Ru_{10}$ exhibits the peak methanol oxidation currents (see Figure 5 in ref 44).

Composition−Activity Trends for Ternaries. Figure 3 reports catalytic activity−composition maps of the chronoamperometric screening of the Pt−Co−Ru focus library. Figure 3a encodes the catalyst activity as the size of the black balls, while the position of the balls marks the initial composition of the catalysts. The Figure also marks the $Pt_{20}Co_{60}Ru_{20}$ alloy from the discovery library by a gray circle. Figure 3b directly correlates overall initial catalyst composition and activity. Figure 3 shows that several catalysts neighboring the $Pt_{20}Co_{60}Ru_{20}$ alloy (highlighted inside the dotted eclipse) did, in fact, exhibit a significantly higher activity than pure Pt as predicted from the discovery library in ref 1.

Except the channels around the discovery composition, most other channels exhibited activities in the 1−10 μA/cm^2 range comparable to pure Pt. The pure Pt benchmark catalyst exhibited a final current density of 2.6 μA/cm^2 after 5 min. These Pt currents agree favorably with an earlier study[63] on sputtered Pt where the initial methanol oxidation current density at the potential of interest was about 10 μA/cm^2 and dropped after 5 min to about 3 μA/cm^2 under otherwise comparable conditions.

Alloys with improved catalytic activity compared to pure Pt split in three groups. One group of alloys (activity >100 μA/cm^2 after 5 min) exhibited significant increases in electrochemical surface areas after screening from initially about 0.02 cm^2 to values of around 0.5–0.7 cm^2. That corresponds to a surface increase of more than 30 times and is attributable to severe surface roughening and metal corrosion. This surface area increase is consistent with the observed activity increases. Examples of this group are $Pt_{17}Co_{73}Ru_{10}$, $Pt_{11}Co_{72}Ru_{17}$, or $Pt_8Co_{72}Ru_{20}$. In line with previous results,[1] all of these channels contain a high combined molar fraction in Co and Ru, which reduced their

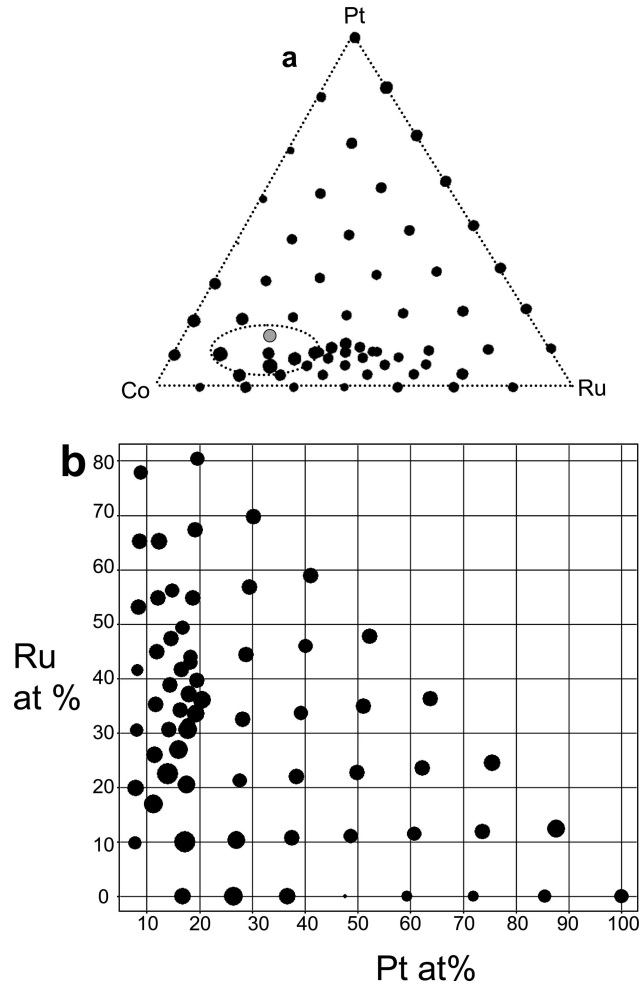

Figure 3. (a) Activity−composition map of the Pt−Co−Ru focus library after 5 min testing (+550 mV/RHE, 1 M methanol, 0.5 M H_2SO_4 electrolyte). (b) Activity−composition map of the Pt−Co−Ru focus library in a rectangular compositional coordinate system. Both maps encode activity by size of the black circles on a logarithmic scale.

electrochemical corrosion stability during cyclic voltammetric pretreatment. A second group of alloys exhibited as high activities as the first group, yet showed small surface area changes. This group of alloys consisted of, among others, $Pt_{14}Co_{63}Ru_{23}$ and $Pt_{16}Co_{57}Ru_{27}$. A third group of alloy catalysts with activities ranging from 30 to 100 μA/cm^2 (10–30 times activity improvements over pure Pt) comprised $Pt_{14}Co_{52}Ru_{30}$ and $Pt_{18}Co_{62}Ru_{20}$. These channels do not show any significant increase in catalyst surface area indicating limited corrosion and therefore acceptable stability. All other channels exhibited activities comparable to pure Pt with or without increased surface area. These latter channels were not further considered.

The observed activity patterns in the Pt−Co−Ru system are in excellent agreement with room temperature measurements of sputtered Pt−Co−Ru thin film methanol electrocatalysts performed by Cooper and McGinn.[44] These authors reported that a $Pt_{17}Co_{66}Ru_{17}$ catalyst outperformed all other composition at room temperature (Figure 8 in ref 44). Their ternary sampling design of the Pt−Co−Ru compositional space was fairly sparse around this composition, which led them to resort to interpolation to determine the compositional extent of optimal catalysts. Their extrapolated compositional

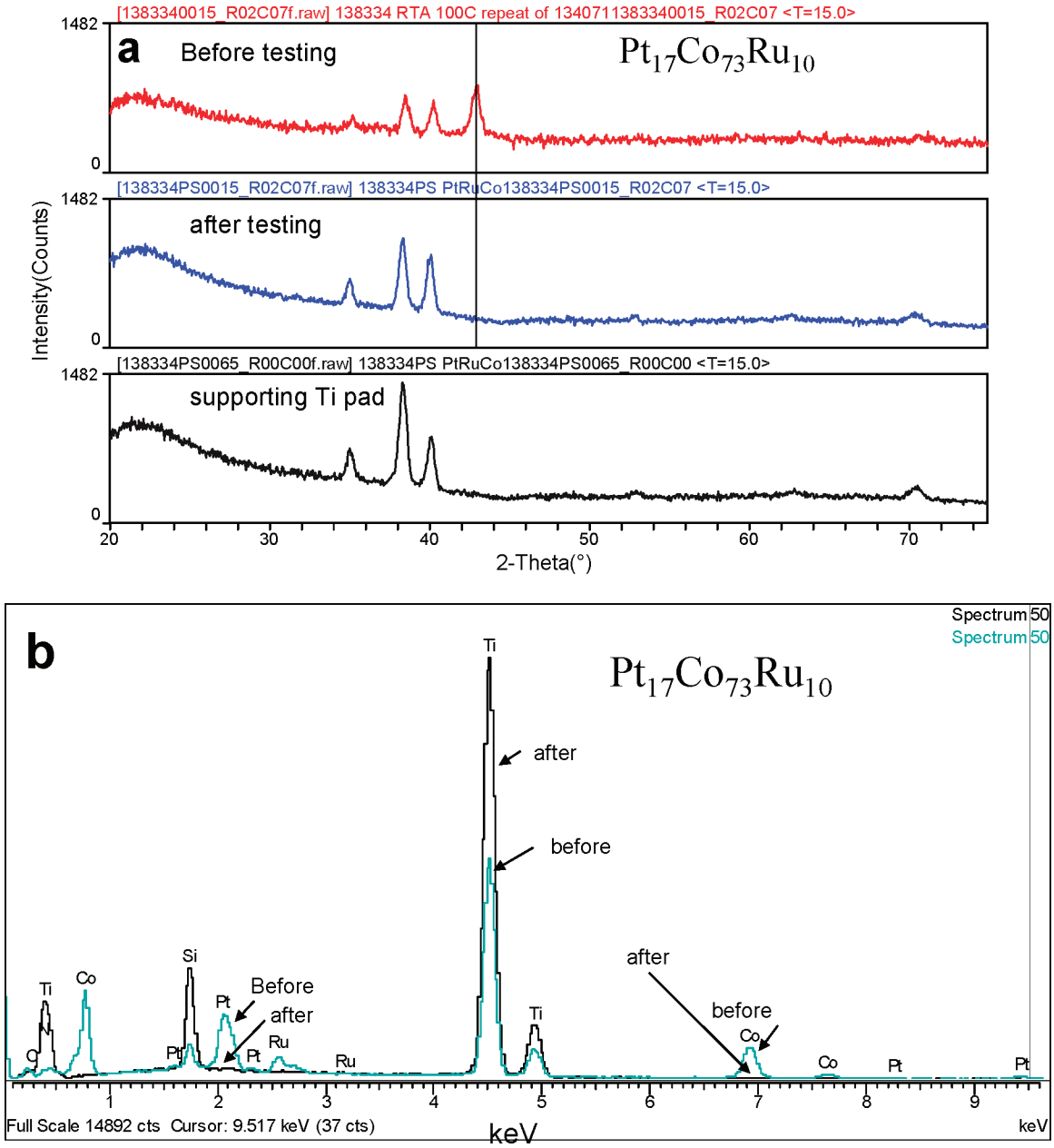

Figure 4. (a) X-ray diffraction profile of the $Pt_{17}Co_{73}Ru_{10}$ alloy thin film before (top profile) after (center profile) testing. The bottom profile represents the Ti supporting electrode. (b) Energy dispersive X-ray spectrum (EDX) of the catalyst before and after screening. Both stability tests indicate severe corrosion of this composition.

space of highest activity comprises exactly the compositions of the most active first group of channels observed in the present study. Also, in line with our observations here, Cooper and McGinn reported the optimal catalyst composition to shift to Co poorer composition as the activity screening was repeated. As expected from the earlier discussion on Pt−Ru binary catalysts, the composition with the highest catalytic activity in ref 44 shifted from $Pt_{17}Co_{66}Ru_{17}$ to more Ru-rich compositions (optimal range in ref 44 was interpolated to be $Pt_{10-20}Ru_{30-50}Co_{30-60}$) as the screening temperature was increased to 60 °C. We suspect that, apart from corrosion changes, changes in the methanol chemisorption characteristics of Ru plays a key role in this shift in activity maximum.

Lima et al.[69] reported a 2 times increase in activity in methanol electrooxidation on Pt−Co−Ru electrocatalysts, yet did not provide much detailed as to which actual compositions are responsible for the observed activity improvement.

3.2. Detailed Stability Optimization. Methods for Probing Stability. Aside from methanol electrooxidation activity, a viable DMFC anode electrocatalyst must exhibit sufficient corrosion stability with respect to the electrode potentials occurring at the anode of a DMFC. Significant changes in the electrochemical surface area (ESA) of Pt alloy catalysts during voltammetric pretreatment are an indicator for alloy instability, because ESAs of alloys typically increase as constituent metals corrode. On the basis of observed ESA changes, active alloys such as $Pt_{17}Co_{73}Ru_{10}$ appear electrochemically unstable. Compositions such as $Pt_{16}Co_{57}Ru_{27}$ or $Pt_{18}Co_{62}Ru_{20}$ with minimal ESA changes require additional stability tests other than ESA, because surface oxide forma-

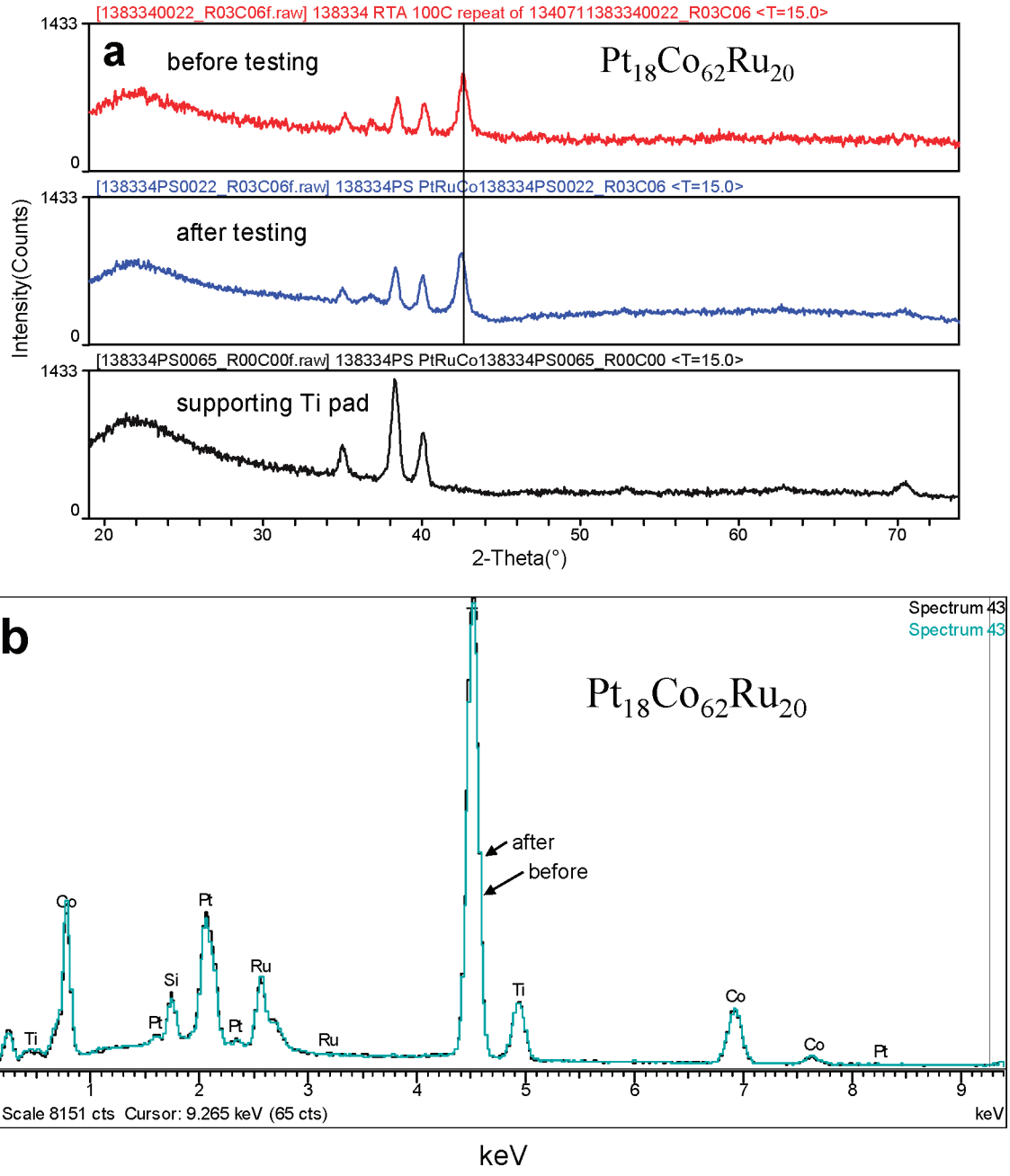

Figure 5. (a) X-ray diffraction profile of the $Pt_{18}Co_{62}Ru_{20}$ alloy thin film before (top profile) after (center profile) testing. The bottom profile represents the Ti supporting electrode. (b) Energy dispersive X-ray spectrum (EDX) of the catalyst before and after screening. Both stability tests indicate good corrosion stability of this composition.

tions, surface restructuring, alloy phase segregation, or alloy phase transformations do not necessarily manifest themselves in ESA changes. This is why more detailed stability criteria were chosen to assess the stability of the active alloys and down select the active catalysts to identify the most optimal candidates.

X-ray diffraction (XRD) profiles and energy-dispersive X-ray analysis spectra (EDX) were used as two independent stability criteria for alloy catalysts on the optimization library. These methods represented the structural and compositional stability, respectively. Alloy stability was associated with time-stable XRD profiles, that is, profiles where all alloy peaks were unchanged in peak position, shape, and height before and after electrochemical testing. Furthermore, alloy catalysts were considered stable if the EDX spectrum indicated identical peak patterns and intensity ratios before and after testing. If catalysts failed to pass either of these two stability criteria, they were considered unstable and were disregarded in the down selection process.

Composition−Stability Maps. Figure 4 shows the structural and compositional characterization of the most active alloy electrocatalyst $Pt_{17}Co_{73}Ru_{10}$ on the focus library. The structural diffraction profile before testing (Figure 4a, top profile) indicates a well-alloyed metal film with a (111) peak position at about $2\theta = 43°$. Reflections at smaller angles are caused by the supporting Ti pad below the catalyst alloy (bottom profile in Figure 4a). After electrocatalytic testing of $Pt_{17}Co_{73}Ru_{10}$, its structural X-ray profile changed significantly. The (111) peak disappeared completely suggesting severe metal solution possibly combined with mechanical

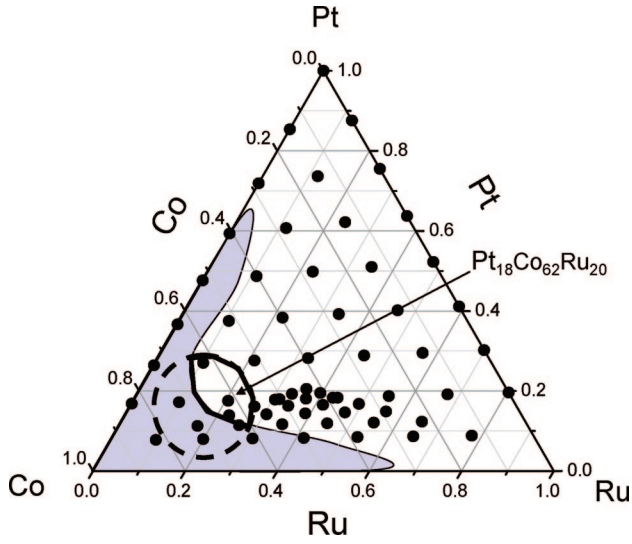

Figure 6. Consensus map of the Pt−Co−Ru focus library superimposing activity and stability maps. The dashed circled region indicates the compositional region of favorable activity, while the gray shaded area represents the compositional region of severe corrosion and instability. The region delineated by the solid black line represents the preferred consensus region. The alloy $Pt_{18}Co_{62}Ru_{20}$ is selected as the lead catalyst on the basis of a balance of activity and stability considerations. It is consistent with the most-active catalyst in the discovery library shown in Figure.4.

detachment of they catalyst film from the Ti pad. Figure 4b shows the EDX spectrum of $Pt_{17}Co_{73}Ru_{10}$ before and after catalytic testing. As expected from the XRD profile, all three metals are absent after electrocatalysis confirming severe corrosion and film destruction. The stability considerations suggest that the alloy $Pt_{17}Co_{73}Ru_{10}$ exhibited very poor electrochemical stability under the chosen catalytic testing conditions, and needs to be discarded from the catalyst down selection process. The likely reason for its instability consists in its relative high combined Ru and Co metal content, which lowered the critical corrosion potential of the alloy to lower electrode potentials.[70–74] The observed transient high catalytic activity is likely caused by methanol oxidation on a severely corroding alloy surface with significantly increased surface area.

Next, the stability of the ternary catalysts $Pt_{16}Co_{57}Ru_{27}$ is considered. This alloy exhibited improved catalytic activity in combination with very small surface area increases after electrocatalysis. Surface area changes cannot be used here as a sufficient condition for electrochemical stability. Inspection of the XRD profile changes of this alloy suggested that the structural stability of the alloy was good, since no changes in peak position or shape was observed for the (111) alloy peak. Inspection of the compositional characteristics of this catalyst, however, indicated that Co metal is selectively dissolved from the catalyst, while Pt and Ru remain in the alloy in their initial relative proportions. Hence, this catalyst, despite its favorable activity and structural characteristics was discarded in the down selection process.

Finally, Figure 5 reports the stability characteristics of the $Pt_{18}Co_{62}Ru_{20}$ alloy which showed significantly improved catalytic activity with no significant change in surface area. Inspection of structural and compositional characteristics in Figure 5a and 5b evidenced that this compositions appeared very stable under the chosen catalytic screening conditions and hence was included in the down selection process.

The stability screenings exemplified in Figures 4 and 5 were applied to all 64 channels using automated sample stages, data acquisition, and data analysis, and full XRD sand EDX stability−composition maps were constructed. Stability borderlines within the ternary composition space where transitions from stability to instability occur were obtained.

Consensus Maps and Final Selection. Combining the activity−composition map with the stability−composition map generated a "consensus map" shown in Figure 6. Here, the compositional range of active compounds near the $Pt_{20}Co_{60}Ru_{20}$ composition (dashed circle) is superimposed with the instability region (gray area) yielding the preferred compositional range of alloy catalysts meeting the activity and stability targets (region bounded by the solid black line). Such consensus plots conveniently facilitate the down selection of suitable preferred lead alloy candidates.

In Figure 6, the $Pt_{18}Co_{62}Ru_{20}$ alloy exhibited the highest methanol electrooxidation activity at acceptable stability inside the activity−stability consensus region. This catalyst constitutes a promising new lead alloy candidate for significant activity enhancement at DMFC anodes. Compared to a pure Pt thin film catalyst, our optimized lead catalyst catalyzed the electrooxidation of methanol about 10× more efficiently.

4. Conclusions

A combinatorial and high throughput exploration of Pt alloy ternary alloy electrocatalysts has been performed. The goal of the study was the rapid identification of improved DMFC methanol electrooxidation catalyst with improved activity and stability characteristics compared to Pt−Ru bimetallics.

An optimization library has been used to screen the Pt−Co−Ru ternary alloy system more closely, in particular in the compositional vicinity of a previously discovered active $Pt_{20}Co_{60}Ru_{20}$ alloy catalyst. Activity trends of the optimization catalyst library were in good agreement with results from fundamental electrochemical studies on Pt−Ru bimetallics, providing evidence for the accuracy of our combinatorial catalyst development workflow. Importantly, the focus library confirmed improved activity in the compositional vicinity of a previously discovered $Pt_{20}Co_{60}Ru_{20}$ alloy composition.[1] A detailed stability evaluation process involving structural and compositional stability criteria pointed to an activity−stability optimum within the consensus map near the composition $Pt_{18}Co_{62}Ru_{20}$.

This study exemplifies the power of combinatorial and high-throughput exploration as a tool to rapidly eliminate a large number of undesirable candidates from a chemical diverse library. Using appropriate selection tools, the remaining materials candidates can be further down selected using consensus maps built from two or more trend maps with respect to a desired materials property. In combination with subsequent fundamental catalyst characterization and computational modeling tools, combinatorial electrocatalyst exploration techniques constitute not only an indispensable tool for rapid materials development breakthroughs but also

guide and focus research efforts on relevant systems that merit fundamental understanding and help develop rational materials design capabilities.

Acknowledgment. The author thanks Dr. Qun Fan, Dr. Daniel Giaquinta, Dr. Konstantinos Chondrudis, Dr. Martin Devenney, Dr. Sasha Gorer, and Prof. Dr. W. Henry Weinberg from the Electronic Materials Group at Symyx Technologies Inc. for their individual support in performing this study. This paper is dedicated to our friend and colleague Keith Cendak whose contributions to this and other studies in terms of synthesis, analytics, and data processing have been significant. We miss him very much.

References and Notes

(1) Strasser, P.; Fan, Q.; Devenney, M.; Weinberg, W. H.; Liu, P.; Norskov, J. K. *J. Phys. Chem. B* **2003**, *107*, 11013.
(2) Vielstich, W., Lamm, A., Gasteiger, H., Eds.; *Handbook of Fuel Cells—Fundamentals, Technology, and Applications*; Wiley: Chichester, U.K., 2003.
(3) Busby, R. L. *Hydrogen and Fuel Cells*; Pennwell Corporation: Tulsa, OK, 2005.
(4) McGrath, K. M.; Prakash, G. K. S.; Olah, G. A. *J. Ind. Eng. Chem.* **2004**, *20*, 1063–1080.
(5) Cropper, M. A. J.; Geiger, S.; Jollie, D. M. *J. Power Sources* **2004**, *131*, 57–61.
(6) Dyer, C. K. *J. Power Sources* **2002**, *106*, 31–34.
(7) Dubois, J. C. *Actual. Chim.* **2001**, *12*, 58–62.
(8) Larminie, J.; Dicks, A. *Fuel Cell Systems Explained*; Wiley: New York, 2000.
(9) O'Hayre, R.; Cha, S.-W.; Colella, W.; Prinz, F. B. *Fuel Cell Fundamentals*; Wiley: New York, 2006.
(10) Li, X. *Principles of Fuel Cells*; Taylor - Francis: New York, 2006.
(11) Lipkowski, J.; Ross, P. N. *Electrocatalysis*; Wiley-VCH: New York, 1998.
(12) Demirci, U. B. *J. Power Sources* **2007**, *173*, 11–18.
(13) Hamnett, A. *Catal. Today* **1997**, *38*, 445.
(14) Kabbabi, A.; Faure, R.; Durand, R.; Beden, B.; Hahn, F.; Leger, J. M.; Lamy, C. *J. Electroanal. Chem.* **1998**, *444*, 41–53.
(15) Shukla, A. K.; Raman, R. K. *Annu. Rev. Mater. Res.* **2003**, *33*, 155–168.
(16) Spendelow, J. S.; Wieckowski, A. *Phys. Chem. Chem. Phys.* **2004**, *9*, 5094–5118.
(17) Spendelow, J. S.; Wieckowski, A. *Phys. Chem. Chem. Phys.* **2007**, *9*, 2654–2675.
(18) Thompsett, D. In *Fuel Cell Technology Handbook*, CRC Press LLC: London, 2003; Chapter 6.
(19) Wasmus, S.; Kuver, A. *J. Electroanal. Chem.* **1999**, *461*, 14–31.
(20) Waszczuk, P.; Gulon, J. S.; Kim, H. S.; Tong, Y. Y.; Montiel, V.; Aldaz, A.; Wieckowski, A. *J. Catal.* **2001**, *203*, 1–6.
(21) Stamenkovic, V.; Moon, B. S.; Mayerhofer, K. J.; Ross, P. N.; Markovic, N.; Rossmeisl, J.; Greeley, J.; Norskov, J. K. *Angew. Chem., Int. Ed.* **2006**, *45*, 2897–2901.
(22) Smotkin, E. S.; Diaz-Morales, R. R. *Annu. Rev. Mater. Res.* **2003**, *33*, 557.
(23) Smotkin, E. S.; Jiang, J.; Nayar, A.; Liu, R. *Appl. Surf. Sci.* **2006**, *252*, 2573–2579.
(24) Hagemeyer, A., Strasser, P., Volpe, A. F., Eds.; *High-Throughput Screening in Chemical Catalysis—Technologies, Strategies and Applications*; Wiley VCH: Weinheim, Germany, 2004.
(25) Archibald, B.; Bruemmer, O.; Devenney, M.; Gorer, A.; Jandeleit, B.; Uno, T.; Weinberg, W. H.; Weskamp, T. In *Handbook of Combinatorial Chemistry—Drugs, Catalyst, Materials*; Nicolaou, K. C., Hangko, R., Hartwig, W., Eds.; Wiley: New York, 2002.
(26) Hagemeyer, A.; Jandeleit, B.; Liu, Y.; Poojary, D. M.; Turner, H. W.; Volpe, A. F.; Weinberg, H. *Appl. Catal. A: General* **2001**, *221*, 23–43.
(27) Jandeleit, B.; Schaefer, D. J.; Powers, T. S.; Turner, H. W.; Weinberg, W. H. *Angew. Chem., Int. Ed. Engl.* **1999**, *38*, 2495–2532.
(28) Mallouk, T. E.; Reddington, E.; Pu, C.; Ley, K. L.; Smotkin, E. S. In *Extended Abstracts*, Fuel Cell Seminar, Orlando, FL, Nov. 17–20 1996; Fuel Cell Seminar Headquarters, Courtesy Associates: Washington, DC, 1996; p 686.
(29) Mallouk, T. E.; Smotkin, E. S. In *Handbook of Fuel Cells—Fundamentals, Technology and Applications*; Vielstich, W., Lamm, A., Gasteiger, H., Eds., John Wiley & Sons: Chichester, U.K., 2003; Vol. 2, Part 3, p 334.
(30) Reddington, E.; Sapienza, A.; Gurau, B.; Viswanathan, R.; Sarangapani, S.; Smotkin, E. S.; Mallouk, T. E. *Science* **1998**, *280*, 1735–1737.
(31) Strasser, P.; Gorer, S.; Devenney, M. In *Proceedings Volume of the International Symposium on Fuel Cells for Vehicles—41st Battery Symposium*; Yamamoto, O., Ed., The Electrochemical Society of Japan: Nagoya, Japan, 2000; p 153.
(32) Strasser, P.; Gorer, S.; Devenney, M. In *Direct Methanol Fuel Cells*; Narayanan, S. R., Zawodzinski, S. G. T., Eds.; The Electrochemical Society: Washington, DC, 2001; Vol. 2001–4, p 191.
(33) Xiang, X.-D.; Sun, X.; Briceno, G.; Lou, Y.; Wang, K.-A.; Chang, H.; Wallace-Freedman, W. G.; Chen, S.-W.; Schultz, P. G. *Science* **1995**, *268*, 1738–1740.
(34) Cooper, J. S.; McGinn, P. J. *Appl. Surf. Sci.* **2007**, *254*, 662–668.
(35) He, T.; Kreidler, E.; Xiong, L.; Ding, E. *ECS Trans.* **2007**, *2*, 13.
(36) He, T.; Kreidler, E.; Xiong, L.; Luo, J.; Zhong, C. J. *J. Electrochem. Soc.* **2006**, *153*, A1637–A1643.
(37) Reddington, E.; Yu, J.-S.; Chan, B. C.; Sapienza, A.; Chen, G.; Mallouk, T. E.; Gurau, B.; Viswanathan, R.; Liu, R.; Smotkin, E. S.; Sarangapani, S. In *Combinatorial Chemistry*; Fenniri, H., Ed., Oxford University Press: Oxford, U.K., 2000; p 401.
(38) Chen, G.; Delafuente, D. A.; Sarangapani, S.; Mallouk, T. E. *Catal. Today* **2001**, *67*, 341–355.
(39) Yamada, Y.; Ueda, A.; Shioyama, H.; Kobayashi, T. *Appl. Surf. Sci.* **2004**, *223*, 220–223.
(40) Choi, W. C.; Kim, Y. J.; Woo, S. I. *Catal. Today* **2002**, *74*, 235.
(41) Choi, W. C.; Kim, Y. J.; Woo, S. I.; Hong, W. H. In *Science and Technology in Catalysis*; Kadansha Ltd: Tokoyo, Japan, 2002; Chapter 86, p 395.
(42) Whitacre, J. F.; Valdez, T.; Narayanan, S. R. *J. Electrochem. Soc.* **2005**, *152*, A1780–A1789.
(43) Reddington, E.; Yu, J.-S.; Sapienza, A.; Chan, B. C.; Gurau, B. *Mater. Res. Soc. Symp. Proc.* **1999**, *549*, 231–236.
(44) Cooper, J. S.; McGinn, P. J. *J. Power Sources* **2006**, *163*, 330–338.
(45) Greeley, J.; Jaramillo, T.; Bonde, J.; Chorkendorff, I.; Nørskov, J. K. *Nat. Mater.* **2006**, *5*, 909–913.
(46) Gorer, A. Platinum—ruthenium—palladium alloys for use as a fuel cell catalyst. U.S. patent 6,498,121, 2002.
(47) Gorer, A. Method for producing electricity using a platinum—ruthenium—palladium catalyst in a fuel cell. U.S. patent 6,682,837, 2004.
(48) Gorer, A. Platinum—ruthenium—nickel alloy for use as a fuel cell catalyst. U.S. patent 6,517,965, 2003.
(49) Kandoi, S.; Greeley, J.; Sanchez-Castillo, M.; Evans, S.; Gokhale, A.; Dumesic, J. A.; Mavrikakis, M. *Top. Catal.* In press.
(50) Cao, D.; Lu, G.-Q.; Wieckowski, A.; Wasileski, S. A.; Neurock, M. *J. Phys. Chem. B* **2005**, *109*, 11622–11633.
(51) Rahim, M. A. A.; Hameed, R. M. A.; Khalil, M. W. *J. Power Sources* **2004**, *135*, 42–51.

(52) Batista, E. A.; Malpass, G. R. P.; Motheo, A. J.; Iwasita, T. *J. Electroanal. Chem.* **2004**, *571*, 273–282.
(53) Greeley, J.; Mavrikakis, M. *J. Am. Chem. Soc.* **2004**, *126*, 3910–3919.
(54) Batista, E. A.; Malpass, G. R. P.; Motheo, A. J.; Iwasita, T. *Electrochem. Commun.* **2003**, *5*, 843–846.
(55) Chen, Y. X.; Miki, A.; Ye, S.; Sakai, H.; Osawa, M. *J. Am. Chem. Soc.* **2003**, *125*, 3680–3681.
(56) Greeley, J.; Mavrikakis, M. *J. Am. Chem. Soc.* **2002**, *124*, 7193–7201.
(57) Diekhöhner, L.; Butler, D.; Baurichter, A.; Luntz, A. *Surf. Sci.* **1998**, *409*, 384–391.
(58) Markovic, N. M.; Gasteiger, H. A., Jr.; P., N. R.; Jiang, X.; Villegas, I.; Weaver, M. J. *Electrochim. Acta* **1995**, *40*, 91–98.
(59) Stamenkovic, V.; Schmidt, T. J.; Ross, P. N.; Markovic, N. M. *J. Phys. Chem. B* **2002**, *106*, 11970–11979.
(60) Stamenkovic, V.; Schmidt, T. J.; Ross, P. N.; Markovic, N. M. *J. Electroanal. Chem.* **2003**, *554*, 191–199.
(61) Bonakdarpour, A.; Wenzel, J.; Stevens, D. A.; Sheng, S.; Monchesky, T. I.; Lobel, R.; Atanasoski, R. T.; Schmoeckel, A. K.; Vernstrom, G. D.; Debe, M. K.; Dahn, J. R. *J. Electrochem. Soc.* **2005**, *152*, A61.
(62) Hatchard, T. D.; Topple, J. M.; Fleischauer, M. D.; Dahn, J. R. *Electrochem. Solid-State Lett.* **2003**, *6*, A129–A132.
(63) Gasteiger, H. A.; Markovic, N. J.; Ross, P. N.; Cairns, E. J. *J. Phys. Chem.* **1993**, *97*, 12020–12029.
(64) Gasteiger, H. A., Jr.; Ross, P. N.; Cairns, E. J. *Surf. Sci.* **1993**, *293*, 67–80.
(65) Gasteiger, H. A.; Markovic, N.; Ross, P. N. *J. Phys. Chem.* **1995**, *99*, 16757–16767.
(66) Gasteiger, H.; Markovic, N.; Ross, P. N. *J. Phys. Chem.* **1995**, *99*, 8290–8301.
(67) Gasteiger, H. A.; Marcovic, N.; Ross, P. N.; Cairns, E. J. *J. Electrochem. Soc.* **1994**, *141*, 1795–1803.
(68) Watanabe, M.; Motoo, S. *J. Electroanal. Chem.* **1975**, *60*, 267–273.
(69) Lima, A.; Coutanceau, C.; Leger, J. M.; Lamy, C. *J. Appl. Electrochem.* **2001**, *31*, 379–386.
(70) Newman, R. C.; Sieradzki, K. *Science* **1994**, *263*, 1708–1709.
(71) Williams, D. E.; Newman, R. C.; Song, Q.; Kelly, R. G. *Nature* **1991**, *350*, 216–219.
(72) Sieradzki, K.; Corderman, R. R.; Shukla, K.; Newman, R. C. *Philos. Mag. A* **1989**, *59*, 713–746.
(73) Pickering, H. W. *Corros. Sci.* **1983**, *23*, 1107–1120.
(74) Pickering, H. W.; Wagner, C. *J. Electrochem. Soc.* **1967**, *114*, 698.

CC700166P